Published in final edited form as:
Nat Struct Mol Biol. 2018 January ; 25(1): 37–44. doi:10.1038/s41594-017-0003-7.

CryoEM structures of the human INO80 chromatin remodelling complex

Ricardo J. Aramayo[1], **Oliver Willhoft**[1], **Rafael Ayala**, **Rohan Bythell-Douglas**, **Dale B. Wigley**[*], and **Xiaodong Zhang**[*]
Section of Structural Biology, Dept. Medicine, Imperial College London, South Kensington Campus, London SW7 2AZ, U.K.

Abstract

Access to chromatin for processes such as DNA repair and transcription requires the sliding of nucleosomes along DNA. The multi-subunit INO80 chromatin remodelling complex has a particular role in DNA repair. Here we present the cryo electron microscopy structures of the active core complex of human INO80 at 9.6 Å with portions at 4.1 Å resolution along with reconstructions of combinations of subunits. Together these structures reveal the architecture of the INO80 complex, including Ino80 and actin-related proteins, which is assembled around a single Tip49a (RUVBL1) and Tip49b (RUVBL2) AAA+ heterohexamer. An unusual spoked-wheel structural domain of the Ino80 subunit is engulfed by this heterohexamer and the intimate association of this Ino80 domain with the heterohexamer is at the core of the complex. We also identify a cleft in RUVBL1 and RUVBL2, which forms a major interaction site for partner proteins and likely communicates partner-interactions with its nucleotide binding sites.

Nucleosome remodelling plays a vital role in almost every transaction involving DNA in eukaryotic cells and can involve covalent modifications, replacement of histones or repositioning of histones on DNA1. Complexes that slide nucleosomes are built around an ATP-dependent translocase motor2 combined with accessory domains or proteins that are involved in recognizing the nucleosome substrate. Some are as simple as a single subunit (e.g. Chd13), others contain a few subunits (e.g. ISWI4), while some are much larger (>1MDa) complexes (e.g. RSC5 and INO806) with multiple subunits, including actin, actin-related proteins (ARPs) and other subunits of unknown function.

The human and yeast INO80 complexes have been studied using proteins expressed at endogenous levels from their respective original hosts6–9. In addition to the main Ino80 motor, the complex contains a conserved core of proteins together with at least half a dozen species-specific subunits of varying functions1. In the human complex, these accessory

[*]Joint corresponding authors.
[1]Joint first authors

Author contributions: DBW and XZ designed and supervised the studies. RJA and RA performed the cryoEM analysis. OW and RBD prepared and biochemically characterised the samples. RBD, RJA and OW built and refined the structural models. DBW and XZ wrote the manuscript with input from all the authors.

The authors declare no competing financial interest.

Europe PMC Funders Author Manuscripts

subunits all interact with the N-terminal region of the Ino80 subunit and are not required for nucleosome-sliding activity9,10. A core complex comprising a truncated Ino80 subunit (residues 267-1556), actin, Arp4, Arp5, Arp8, Ies2, Ies6, Tip49a (also known as RUVBL1), Tip49b (RUVBL2) is fully active and can be made recombinantly in insect cells10.

RUVBL1 and RUVBL2 belong to the large AAA+ protein family11 and are components of several complexes involved in a diverse range of biological functions11,12. However, their precise role in these complexes remains unknown. There are a number of high and medium resolution structures of RUVBL1 and RUVBL2 homologues in isolation13–17 and low resolution electron microscopy reconstructions of yeast RUVBL1 and RUVBL2 in the context of INO80 or SWR118,19. However, the lack of high-resolution structural information for RUVBL1 and RUVBL2 in the context of larger complexes prevents detailed analysis of their biological function, conformation and interactions with their binding partners.

Here we present the structure of a human INO80 core complex9,10,20 at 9.6 Å with portions at 4.1 Å resolution. This core complex was previously shown to have nucleosome sliding activity comparable to the full complex *in vitro*. The structure contains a single RUVBL1 and RUVBL2 heterohexamer (termed RUVBL1-2 hereafter) with alternating subunits. The complex is conformationally flexible, with arms extending from the RUVBL1-2 ring. Each RUVBL1 and RUVBL2 monomer makes extensive and unique interactions with the Ino80 subunit and other subunits within the INO80 complex. A large insertion within the Ino80 helicase domain forms a spoked-wheel structure that is enclosed entirely within a barrel formed by the RUVBL1-2 hexamer. We have also identified a novel cleft in RUVBL1 and RUVBL2, which acts as a major Ino80 interaction site and likely communicates partner interactions to the AAA+ domain of RUVBL1-2.

Results

CryoEM structures of hINO80 core, SC2 and SC2plus complexes

Previously, a low resolution EM structure of the yeast INO80 complex suggested there were two RUVBL1-2 heterohexamers (a RUVBL1-2 dodecamer) present in the yeast INO80 complex19. However, the limited resolution of the reconstruction prevented an accurate assignment of subunits and domains. Here, we have obtained structures of several subunit combinations of the human INO80 complex at resolutions from ~12 Å to 4.1 Å, using cryoEM (Fig.1, Supplementary Figs. 1-2 and Table 1).

Similar to the related SWR1 complex18,21, the hINO80 core complex exhibits considerable conformational flexibility. 2D classification highlighted the presence of strong density corresponding to a single RUVBL1-2 hexamer, to which a tail is attached (Supplementary Fig. 1a). However, the particle size of the class averages is smaller than that expected for the hINO80 core complex despite all the subunits being present after protein purification10. We reasoned that either some subunits had dissociated or there are conformationally flexible regions relative to the RUVBL1-2 hexamer and therefore the corresponding density has been averaged out. Consequently, we further examined the 2D classes carefully (Supplementary Fig. 2a) and identified a small population of particles (~5-10%) with additional density

(Supplementary Fig. 2a circles). However, the strong signal of the AAA+ ring in cryoEM images (Supplementary Fig. 1a & 2a) dominates the alignment during subsequent image processing, resulting in the loss of information for conformationally mobile regions that are spatially remote from the ring. To address this issue, we selected particles with clear additional density and performed multiple rounds of rigorous 2D classification to select a population of similar conformation. After multiple rounds of 3D classification and refinement in cryoSPARC22, a reconstruction at 9.6 Å was obtained from ~11,000 particles (Fig. 1a). The reconstruction contains two distinct components: a strong hexameric feature comprising approximately two-thirds of the molecular mass, and a smaller part that is tethered to the larger part via a region of very thin connecting density. This is in good agreement with the distribution of mass within the hINO80 core complex10. We refer to this structure as the hINO80 core complex hereafter.

The whole dataset (~300,000 particles) was processed in RELION23 through multiple rounds of 3D classification and refinement. The final structure (Fig. 1b) is based on ~100,000 particles and has an overall resolution of 4.1 Å (Supplementary Fig. 1 and Table 1). A clear, single hexameric ring is evident with additional density below and on the side of the ring (Fig. 1b). This high-resolution reconstruction resembles the upper half of the lower resolution hINO80 core reconstruction, confirming our hypothesis that the additional component of the complex is either dissociated or flexible and is thus averaged out during image processing. For clarity, we subsequently refer to the 4.1 Å resolution reconstruction as the high-resolution hINO80 core sub-complex.

Subunit assignments

We used structures of two other hINO80 sub-complexes containing the RUVBL1-2 hexamer to determine the location of subunits within these reconstructions. A C-terminal region (residues 521-1556) of the hIno80 subunit forms a stable complex with RUVBL1-2, Arp5 and Ies69,10, while the helicase-SANT-associated (HSA) module (residues 273-404) recruits Arp8, actin, Arp4 (sub-complex 1, SC1, Fig. 2a)9**.** These interactions are the same in yeast INO8024,25. We obtained reconstructions containing a C-terminal fragment of Ino80 (residues 487-1556) in complex with RUVBL1-2, which we termed sub-complex 2 (SC2), or SC2 together with Arp5-Ies6 and Ies2, which we termed SC2plus (Fig. 2a, Supplementary Fig. 2). Despite the limited resolution of these two reconstructions (11.5 Å and 8.4 Å, respectively, Supplementary Fig. 2), they remain consistent with the presence of a single RUVBL1-2 heterohexamer but with additional density to account for the other co-expressed subunit(s) (Fig. 1 and Supplementary Fig. 2). A comparison of the SC2 and SC2plus structures shows the main difference is the presence of the tail density in SC2plus. Arp5 and Ies6 are known to form a stable heterodimer10,26,27 and the size of the tail suggests that it can accommodate Arp5-Ies6 but is too large for Ies2 alone. We thus assign the tail to be Arp5-Ies6, which is also confirmed by the high resolution INO80 core sub-complex (see below).

In the hINO80 core complex structure, there is an additional density not present in SC2 or SC2plus. We therefore assigned this part as SC1 (Fig. 2a & 2b). Biochemical and genetic data show that when Arp8 is deleted, both actin and Arp4 are lost, while when actin is

deleted, Arp4 can no longer be recruited10,24. This suggests an organisation of Arp8 followed by actin and then Arp4. Indeed, we could fit the actin-Arp4-HSA crystal structure from the related yeast SWR1 system28 into one end of the density, leaving the remaining density for Arp8 although we cannot rule out other alternative arrangements (Fig. 2). We have previously determined a crystal structure of the C-terminal actin-related portion of yeast Arp8, which is equivalent to the shorter human Arp8 protein29 and we could fit an Arp8 monomer into the density (Fig. 2b).

Model building in the high-resolution Ino80 core sub-complex structure

With the assignment of Arp5-Ies6 and SC1, there are additional regions of density below and on the side of the RUVBL1-2 hexameric ring in all of the reconstructions that could account for Ino80 and/or Ies2 (Figs. 1 and 2). To obtain the exact locations and interactions of the Ino80 subunit, we built a number of structural models with variable degrees of detail into the hINO80 reconstructions (Fig. 2). RUVBL1 and RUVBL2 consist of three domains (Fig. 3a). DI and DIII form the AAA+ domain while DII, an insertion into the AAA+ domain, consists of an α-helical region, a long and flexible β-stalk and an oligonucleotide/oligosaccharide binding (OB) fold. Density was observed for DI and DIII as well as most of DII, with secondary structure elements and some side chains clearly resolved (Fig. 3, Supplementary Fig. 1c). RUVBL1 has a longer insertion in the DII helical bundle (Supplementary Note) and we used this feature, along with side chain densities, to clearly distinguish RUVBL1 from RUVBL2. We used the crystal structures of human RUVBL1 and RUVBL2 (PDB codes 2C9O and 2XSZ) as well as homology models generated from the *C. thermophilum* (Ct) RUVBL1/2 heterohexamer (4WW4) to guide our model building13,16,17 and performed a round of refinement against the high-resolution map (Table 1). Although the DII domains adopt a variety of conformations in crystal structures, in our structure they all extend downwards (Fig. 3b).

Density below the AAA+ ring extends downwards ~60 Å, with an elongated tail to the side (Fig. 3b). The resolution for this part of the structure is lower (5-7 Å, Supplementary Fig. 1b), likely reflecting its flexible nature. We also generated a difference map by removing density corresponding to the built model of RUVBL1-2, that comprises a flat disk sitting under the RUVBL1-2 AAA+ domain with additional density extending downwards (Fig. 3c). This accounts for Arp5-Ies6, Ino80 and Ies2.

The reconstructions of SC2 and SC2plus suggest that the tail density corresponds to the Arp5-Ies6 heterodimer (Fig. 1c & 1d). In agreement with this assignment, we could place the coordinates for an actin fold into this region of the hINO80 core sub-complex reconstruction (Fig. 3d, supplementary Fig. 3). There is additional density between the Arp5 and the OB folds of the adjacent RUVBL1 and RUVBL2 (Fig. 3d). Crosslinking mass spectrometry has shown that Ies6 can be crosslinked to both Arp5 and the OB fold of both RUVBL1 and RUVBL2, but there are no observed crosslinks between Arp5 and the complex other than to Ies619. It is therefore likely that this extra density region corresponds to Ies6 and/or the regions of Arp5 that are additional to the actin core.

The extra density inside the RUVBL1-2 barrel, as well as that connected to it (Fig. 3c), thus corresponds to the Ino80 and Ies2 subunits. In Ino80, there is a large insertion within the

helicase domain (Ino80-I), which is known to interact with the RUVBL1-2 proteins (Fig. 2a)30,9. Aside from the helicase and HSA domains of Ino80, there is no structural information available for other regions of Ino80, although secondary structure predictions31 suggest that Ino80-I bears some α-helices flanked by largely loop/coil regions. We reasoned that the flat, wheel-like density encapsulated by the RUVBL1-2 barrel (Fig. 3c) corresponds to Ino80-I for the following reasons: (i) biochemical data show that this insertion region contains the main interaction sites for RUVBL1-230, (ii) the Ino80 helicase domains bind to nucleosomes so must be positioned on the periphery of the complex, and (iii) the Ino80 C-terminal domain (Ino80-C) and Ies2 can be deleted without affecting the assembly of the complex9,20. This assignment is also consistent with a recent low-resolution EM study of a complex between the yeast Ino80-I domain bound to a RUVBL1/2 complex32.

The Ino80-I domain resembles a spoked-wheel with density that follows the inner contour of the RUVBL1-2 β-stalks and spokes linking different regions across the circle (Fig. 3c & 4a). Due to the relatively low resolution (~ 4.1-4.5 Å) and lack of reliable structural models, we only placed a few α-helices into some of the density. Nevertheless, the RUVBL1-2 clearly engulfs the Ino80-I domain, explaining the absolute requirement of RUVBL1-2 for expression of the INO80 complex10. The spoked-wheel structure of Ino80-I suggests that it has a relatively rigid architecture once formed, which could restrain the conformation of the RUVBL1-2 DII domains that wrap around the wheel (Fig. 3c).

Having established the locations of SC1, RUVBL1-2, Ino80-I and Arp5-Ies6 in the reconstruction, the remaining unassigned density regions in the hINO80 core complex and the sub-complexes must contain Ino80-H, Ino80-C and Ies2 (Fig. 4b). After subtracting density corresponding to RUVBL1-2 in the high resolution hINO80 core sub-complex reconstruction, there are two regions of density connected to Ino80-I. Since Ino80-I is an insertion into the C-terminal RecA fold of the Ino80-H domain (referred to as Ino80-HC with the N-terminal RecA fold as Ino80-HN), we reason that one of these regions of density is Ino80-HC (Fig. 4c). One of these density regions is also present in the difference map between SC2 and SC2plus, suggesting that this is Ies2 (Fig. 4c, mesh). This leaves the density on the side of the RUVBL1-2 ring to be Ino80-HC (Fig. 4c). These density regions are also present in the hINO80 core complex, which has additional density just below the RUVBL1-2 ring and above SC1 (Fig. 4d). We suggest that in this reconstruction, Ino80-HN likely resides in this region due to its proximity to SC1. In the Chd1, Snf2 and ISWI structures33–35, as for other SF2 helicase/translocases2, the two RecA-like folds of the motor domain have considerable conformational flexibility and crystallise with highly variable relative orientations, suggesting that this could be one source of the conformational flexibility observed in the INO80 core complex structure. It is possible that the flexibility of Ino80-HN relative to Ino80-HC contributes to the lack of SC1 density in the high resolution reconstruction. Whereas the Ino80-HN is in a position that leads to the SC1 being conformationally constrained in the hINO80 core complex structure captured here, the majority of proteins have Ino80-HN in orientations that are different. Crosslinking studies suggest that, in addition to the OB folds of RUVBL1-2, Ies2 is close to both Ino80 RecA domains as well as the HSA domain, which forms part of SC119. The Ies2 position deduced from the difference map between SC2plus and SC2 (Fig. 4c-d) spans all of the components in the hINO80 core complex, and is also in agreement with the crosslinking data. However,

in the absence of high resolution structural information, there remains ambiguity in the exact locations of some subunits.

Structure of the RUVBL1-2 ring and its interaction with Ino80-I

The best-resolved regions within each reconstruction correspond to the RUVBL1 and RUVBL2 proteins and reveals, for the first time, high-resolution structural information of RUVBL1-2 interacting asymmetrically with multiple binding partners in the context of a multisubunit complex. A side view of the RUVBL1-2 heterohexamer broadly shows three layers: the top layer consists of the AAA+ ring formed by DI and DIII (Fig. 3a & 5a), the middle layer comprises the DII helical bundle and β-stalk, while the bottom layer is formed by the OB folds (Fig. 5a). The top layer has very little space around the hexamer axis (Fig. 5b-c), while the β-stalk and the OB folds form a barrel, enclosing a large cavity. The AAA+ ring, rather than showing 3-fold symmetry, instead has pseudo 6-fold symmetry despite being a RUVBL1 and RUVBL2 hetero-hexamer (Fig. 5b) but the symmetry breaks down below the AAA+ ring (Fig. 5c & 4d). Most strikingly, although all six OB domains stretch downwards, they are positioned differently relative to the main AAA+ domain. Despite the absence of added nucleotide during sample purification and preparation, we observe ADP bound in all RUVBL1-2 protomers (Supplementary Fig. 4). Interestingly, despite this, the individual subunits (in particular the RUVBL2 subunits) have different conformations when superimposed on their P-loops, demonstrating conformational plasticity (Supplementary Fig. 5).

RUVBL1-2 and Ino80, together with other subunits, form an intricate network of interactions. Indeed, RUVBL1-2 interacts extensively with the Ino80-I domain, Ino80-HC and other subunits via a wide range of structural features including the DII helical bundle and the β-stalk as well as the OB domains (Fig. 6). All protomers interact with Ino80-I through the DII helical bundle and the β-stalk. Nevertheless, each RUVBL1-2 monomer has distinct partners and interactions, giving rise to a globally asymmetric structure (Fig. 6a). Protomers A (RUVBL1) and B (RUVBL2) interact with Ino80-I through the DII helical bundle and β-stalk, as well as with Arp5-Ies6 through the OB domains (Fig. 6b). Protomers C (RUVBL1) and D (RUVBL2) interact similarly with Ino80-I using the DII helical bundle and β-stalk, but the OB fold of protomer D also interacts with Ies2 (Fig. 6c). Protomer E (RUVBL1) interacts with Ino80-I through a combination of its DII helical bundle, the β-stalk and OB fold, but also forms an important anchor point for Ies2 (Fig. 6c). Protomer F (RUVBL2) binds in a groove formed by the Ino80-I domain (Fig. 6d). RUVBL1-2 therefore acting as a hub, engulfing the Ino80-I domain as well as interacting with several other Ino80 domains and other subunits.

A new partner-binding site in RUVBL1-2

In order to understand how the differences between RUVBL1-2 protomers relate to partner binding, we compared the interactions of Ino80 with individual RUVBL1 and RUVBL2 protomers. We noted that the DII α-helical bundle and the β-stalk in each subunit form a cleft to which Ino80-I binds (Fig. 7a). The cleft is largely hydrophobic at the centre and is structurally flexible, (Fig. 7b, Supplementary Fig. 6). Furthermore, the surrounding regions are more positively charged in RUVBL1 (Figs. 7b-c, Supplementary Figs 6a-c) but more

negatively charged in RUVBL2 (Supplementary Figs. 6d-f), enabling the binding site to accommodate a wide range of structural and sequence features. It is noteworthy that these partner-binding sites are occluded when hexamers associate to form dodecamers as observed in the crystal structures (see below).

Discussion

Comparisons with INO80 family chromatin remodellers

The structures presented here reveal details of the subunit topology of hINO80 and provide insight into the RUVBL1-2 conformations in the context of a large multisubunit complex. INO80 is a member of a group of remodelling complexes that includes the SWR1 histone exchange complex, with which INO80 shares many subunits including actin, Arp4, RUVBL1 and RUVBL21. Low-resolution EM structures together with biochemical data18,21,27 confirm that SWR1 complex contains a single heterohexamer of RUVBL1-2. Both structures also reveal that the RUVBL1-2 proteins themselves adopt an extended conformation in the complex with considerable conformational flexibility of domains that extend from the AAA+ ring, in common with what we observe for hINO80.

Based on a low-resolution cryoEM structure of a glutaraldehyde cross-linked yeast INO80 complex19, it was suggested that INO80 contains a dodecamer of RUVBL1-2 proteins. However, biochemical data have shown that, as in SWR1, there is a single heterohexamer in both the yeast18,27 and human10 INO80 complexes. Although the overall shape of the low resolution yeast structure19 does bear a superficial resemblance to our higher resolution reconstructions, insofar as having a globular “head” with an extended tail region, the similarity is limited to this topology. The subunit assignments differ significantly between the two structures, stemming from the interpretation of the head as containing a RUVBL1-2 dodecamer and, therefore, density corresponding to a large part of the structure is incorrectly assigned as a second RUVBL1-2 hexamer (equivalent to approximately 25% of the mass of the structure). Consequently, the remaining subunit locations are misplaced. Although a model was created that appeared to be consistent with chemical crosslinking and mass spectrometry analysis, we note that the model we present is also consistent with their crosslinking data19.

Comparisons with other RUVBL1-2 structures

There are a number of crystal structures of RUVBL1-2 homo or heterohexamers13,14,16. These structures show strict 6-fold (homohexamer) or 3-fold (heterohexamer) symmetry. In ctRUVBL1-2 crystal structures, irrespective of nucleotide bound, all the ctRUVBL1 DII domains are in extended conformation while the ctRUVBL2 DII are in compact conformation, in stark contrast to what we observe for the RUVBL1-2 heterohexamer in the context of the INO80 core complex, where the DII are all in extended conformations and all monomers differ, even in the AAA+ domains, despite having ADP bound (supplementary Figs. 4-5, supplementary Table 1).

Comparing the ctRUVBL1-2 crystal structures with the RUVBL1-2s in our INO80 complex reveals that the binding cleft in DII is in a more closed conformation in ctRUVBL2

(Supplementary Fig. 7a). This coincides with the compact conformation of the OB domain, which would occupy the same space as Ino80-I (Supplementary Fig. 7b). The cleft in ctRUVBL1 is similar to that of hRUVBL1 and the OB domain is in an extended conformation (Supplementary Fig. 7c). Interestingly, even though there is no partner bound in these structures, the N-terminus of ctRUVBL1 tucks into the cleft, which mimics partner binding and results in opening of the cleft (Supplementary Fig. 7d). These crystal structures, together with the hRUVBL1-2 structures presented here, suggest that the binding cleft and the OB domains synergistically affect the conformations of one another. Indeed, in the ctRUVBL1-2 crystal structures, the OB domains from adjacent hexamers interact with, and stabilise, one another in a tail-to-tail fashion through crystal packing (the extended ctRUVBL1 OB fold from one hexamer interacts with the compact ctRUVBL2 OB fold from another hexamer), limiting the conformational flexibility of the DII cleft and the AAA+ domain, explaining the high similarity of these structures irrespective of whether ADP or ATP is bound.

Comparisons with other AAA+ proteins

The large AAA+ family mainly comprises homohexamers that show an asymmetric arrangement of protomers within the hexamer upon binding to substrate36–40. A number of AAA+ proteins (e.g. VAT unfoldase, Vsp4, MCM and 19S proteasome) have been shown to translocate substrates through the central pore formed by the ring. A sequential mechanism, involving a helical arrangement of central pore loops, has been proposed for these AAA+ proteins36–38. To date, there is no detailed structural information on a heterohexamer with substrate bound. Here, we do not observe a helical arrangement of RUVBL1-2 heterodimers. Importantly, our structure shows that the central pore is very narrow and is therefore unable to accommodate partner proteins or translocate substrates through it. Instead, all the interactions are below the DII helical bundle, in or around the β-barrel, or with the OB domains.

Previously, RUVBL1 and RUVBL2 have been assigned to a AAA+ subgroup containing substrate translocases/proteases such as ClpX and Lon11 that are thought to translocate their substrates through central pore of the ring41. However, the position of the DII domain relative to the AAA+ domain places it more appropriately in the same subgroup as those of bacterial enhancer-binding proteins NtrC and PspF, which have an insertion (L1 loop) into the AAA+ domain at a similar location as those of DII42–44. Indeed, for this family of AAA+ proteins, this insertion has been shown to interact with substrate42,44,45 and there is no evidence to support translocation of substrate through the central pore. Nucleotide states are shown to control the conformation of the insertions and *vice versa*43,46. It is therefore possible that changes in nucleotide binding sites in RUVBL1-2 could induce changes in the DII partner-binding cleft, which could subsequently act on the Ino80-I spoked-wheel structure that is covalently connected to the Ino80 ATPase domain.

RUVBL1 and RUVBL2 act as a chaperone and hub in large assemblies

The structures presented here explain the absolute requirement of RUVBL1-2 in INO80 complex assembly. We reveal a new partner-binding site in RUVBL1-2. The structural plasticity of this site enables RUVBL1-2 to adapt to binding a wide range of features, both

on a structural and sequence level. The structural plasticity of the ADP-bound state in RUVBL1-2 might be important in providing and permitting the binding flexibility that could correlate with the conformational flexibility of OB domains. RUVBL1-2 proteins are components of a number of different protein assemblies with similarities in their function of acting as a chaperone. The structural plasticity and the binding sites revealed here are likely also to play important roles in these alternative complexes. Our structures show how the nucleotide-binding sites of the AAA+ domains are linked to the Ino80-I domain and, through this, to the motor domains of the Ino80 subunit. Exactly how the action of RUVBL1-2 might be linked to the chromatin remodelling activity of INO80 will require structural details of nucleosome-bound complexes, most likely in different nucleotide states.

Supplementary Material

Refer to Web version on PubMed Central for supplementary material.

Acknowledgements

We would like to thank Daniel Clare and Alistair Siebert at eBIC, Diamond Light Source where the data were collected. We thank the members in the Section of Structural Biology for fruitful discussions. The work was funded by the Wellcome Trust Investigator awards 098412/Z/12/Z to XZ and 095519/Z/11/Z to DBW and a Cancer Research UK grant C6913/A21608 to DBW.

References

1. Clapier CR, Cairns BR. The biology of chromatin remodeling complexes. Annu Rev Biochem. 2009; 78:273–304. [PubMed: 19355820]
2. Singleton MR, Dillingham MS, Wigley DB. Structure and mechanism of helicases and nucleic acid translocases. Annu Rev Biochem. 2007; 76:23–50. [PubMed: 17506634]
3. Delmas V, Stokes DG, Perry RP. A mammalian DNA-binding protein that contains a chromodomain and an SNF2/SWI2-like helicase domain. Proc Natl Acad Sci U S A. 1993; 90:2414–8. [PubMed: 8460153]
4. Ito T, Bulger M, Pazin MJ, Kobayashi R, Kadonaga JT. ACF, an ISWI-containing and ATP-utilizing chromatin assembly and remodeling factor. Cell. 1997; 90:145–55. [PubMed: 9230310]
5. Cairns BR, et al. RSC, an essential, abundant chromatin-remodeling complex. Cell. 1996; 87:1249–60. [PubMed: 8980231]
6. Shen X, Mizuguchi G, Hamiche A, Wu C. A chromatin remodelling complex involved in transcription and DNA processing. Nature. 2000; 406:541–4. [PubMed: 10952318]
7. Jin J, et al. A mammalian chromatin remodeling complex with similarities to the yeast INO80 complex. J Biol Chem. 2005; 280:41207–12. [PubMed: 16230350]
8. Cai Y, et al. Purification and assay of the human INO80 and SRCAP chromatin remodeling complexes. Methods. 2006; 40:312–7. [PubMed: 17101442]
9. Chen L, et al. Subunit organization of the human INO80 chromatin remodeling complex: an evolutionarily conserved core complex catalyzes ATP-dependent nucleosome remodeling. J Biol Chem. 2011; 286:11283–9. [PubMed: 21303910]
10. Willhoft O, Bythell-Douglas R, McCormack EA, Wigley DB. Synergy and antagonism in regulation of recombinant human INO80 chromatin remodeling complex. Nucleic Acids Res. 2016; 44:8179–88. [PubMed: 27257055]
11. Erzberger JP, Berger JM. Evolutionary relationships and structural mechanisms of AAA+ proteins. Annu Rev Biophys Biomol Struct. 2006; 35:93–114. [PubMed: 16689629]
12. Nano N, Houry WA. Chaperone-like activity of the AAA+ proteins Rvb1 and Rvb2 in the assembly of various complexes. Philos Trans R Soc Lond B Biol Sci. 2013; 368 20110399.

13. Lakomek K, Stoehr G, Tosi A, Schmailzl M, Hopfner KP. Structural basis for dodecameric assembly states and conformational plasticity of the full-length AAA+ ATPases Rvb1 . Rvb2. Structure. 2015; 23:483–95. [PubMed: 25661652]
14. Silva-Martin N, et al. The Combination of X-Ray Crystallography and Cryo-Electron Microscopy Provides Insight into the Overall Architecture of the Dodecameric Rvb1/Rvb2 Complex. PLoS One. 2016; 11 e0146457.
15. Ewens CA, et al. Architecture and Nucleotide-Dependent Conformational Changes of the Rvb1-Rvb2 AAA+ Complex Revealed by Cryoelectron Microscopy. Structure. 2016; 24:657–66. [PubMed: 27112599]
16. Gorynia S, et al. Structural and functional insights into a dodecameric molecular machine - the RuvBL1/RuvBL2 complex. J Struct Biol. 2011; 176:279–91. [PubMed: 21933716]
17. Matias PM, Gorynia S, Donner P, Carrondo MA. Crystal structure of the human AAA+ protein RuvBL1. J Biol Chem. 2006; 281:38918–29. [PubMed: 17060327]
18. Nguyen VQ, et al. Molecular architecture of the ATP-dependent chromatin-remodeling complex SWR1. Cell. 2013; 154:1220–31. [PubMed: 24034246]
19. Tosi A, et al. Structure and subunit topology of the INO80 chromatin remodeler and its nucleosome complex. Cell. 2013; 154:1207–19. [PubMed: 24034245]
20. Willhoft O, et al. Cross-talk within a functional INO80 complex dimer regulates nucleosome sliding. Elife. 2017; 6
21. Lin CL, et al. Functional characterization and architecture of recombinant yeast SWR1 histone exchange complex. Nucleic Acids Res. 2017
22. Punjani A, Rubinstein JL, Fleet DJ, Brubaker MA. cryoSPARC: algorithms for rapid unsupervised cryo-EM structure determination. Nat Methods. 2017; 14:290–296. [PubMed: 28165473]
23. Scheres SH. RELION: implementation of a Bayesian approach to cryo-EM structure determination. J Struct Biol. 2012; 180:519–30. [PubMed: 23000701]
24. Shen X, Ranallo R, Choi E, Wu C. Involvement of actin-related proteins in ATP-dependent chromatin remodeling. Mol Cell. 2003; 12:147–55. [PubMed: 12887900]
25. Szerlong H, et al. The HSA domain binds nuclear actin-related proteins to regulate chromatin-remodeling ATPases. Nat Struct Mol Biol. 2008; 15:469–76. [PubMed: 18408732]
26. Morrison AJ, et al. INO80 and gamma-H2AX interaction links ATP-dependent chromatin remodeling to DNA damage repair. Cell. 2004; 119:767–75. [PubMed: 15607974]
27. Watanabe S, et al. Structural analyses of the chromatin remodelling enzymes INO80-C and SWR-C. Nat Commun. 2015; 6:7108. [PubMed: 25964121]
28. Cao T, et al. Crystal structure of a nuclear actin ternary complex. Proc Natl Acad Sci U S A. 2016; 113:8985–90. [PubMed: 27457955]
29. Saravanan M, et al. Interactions between the nucleosome histone core and Arp8 in the INO80 chromatin remodeling complex. Proceedings of the National Academy of Sciences of the United States of America. 2012; 109:20883–8. [PubMed: 23213201]
30. Chen L, Conaway RC, Conaway JW. Multiple modes of regulation of the human Ino80 SNF2 ATPase by subunits of the INO80 chromatin-remodeling complex. Proc Natl Acad Sci U S A. 2013; 110:20497–502. [PubMed: 24297934]
31. Kelley LA, Mezulis S, Yates CM, Wass MN, Sternberg MJ. The Phyre2 web portal for protein modeling, prediction and analysis. Nat Protoc. 2015; 10:845–58. [PubMed: 25950237]
32. Zhou CY, et al. Regulation of Rvb1/Rvb2 by a Domain within the INO80 Chromatin Remodeling Complex Implicates the Yeast Rvbs as Protein Assembly Chaperones. Cell Rep. 2017; 19:2033–2044. [PubMed: 28591576]
33. Yan L, Wang L, Tian Y, Xia X, Chen Z. Structure and regulation of the chromatin remodeller ISWI. Nature. 2016; 540:466–469. [PubMed: 27919072]
34. Hauk G, McKnight JN, Nodelman IM, Bowman GD. The chromodomains of the Chd1 chromatin remodeler regulate DNA access to the ATPase motor. Mol Cell. 2010; 39:711–23. [PubMed: 20832723]

35. Zhang D, Li Y, Zhang X, Zha P, Lin R. The SWI2/SNF2 Chromatin-Remodeling ATPase BRAHMA Regulates Chlorophyll Biosynthesis in Arabidopsis. Mol Plant. 2017; 10:155–167. [PubMed: 27865928]
36. Enemark EJ, Chen G, Vaughn DE, Stenlund A, Joshua-Tor L. Crystal structure of the DNA binding domain of the replication initiation protein E1 from papillomavirus. Mol Cell. 2000; 6:149–58. [PubMed: 10949036]
37. Ripstein ZA, Huang R, Augustyniak R, Kay LE, Rubinstein JL. Structure of a AAA+ unfoldase in the process of unfolding substrate. Elife. 2017; 6
38. Monroe N, Han H, Shen PS, Sundquist WI, Hill CP. Structural basis of protein translocation by the Vps4-Vta1 AAA ATPase. Elife. 2017; 6
39. Yuan Z, et al. Structural basis of Mcm2-7 replicative helicase loading by ORC-Cdc6 and Cdt1. Nat Struct Mol Biol. 2017; 24:316–324. [PubMed: 28191893]
40. Schweitzer A, et al. Structure of the human 26S proteasome at a resolution of 3.9 A. Proc Natl Acad Sci U S A. 2016; 113:7816–21. [PubMed: 27342858]
41. Martin A, Baker TA, Sauer RT. Pore loops of the AAA+ ClpX machine grip substrates to drive translocation and unfolding. Nat Struct Mol Biol. 2008; 15:1147–51. [PubMed: 18931677]
42. Rappas M, et al. Structural insights into the activity of enhancer-binding proteins. Science. 2005; 307:1972–5. [PubMed: 15790859]
43. Rappas M, Schumacher J, Niwa H, Buck M, Zhang X. Structural basis of the nucleotide driven conformational changes in the AAA+ domain of transcription activator PspF. J Mol Biol. 2006; 357:481–92. [PubMed: 16430918]
44. Lee SY, et al. Regulation of the transcriptional activator NtrC1: structural studies of the regulatory and AAA+ ATPase domains. Genes Dev. 2003; 17:2552–63. [PubMed: 14561776]
45. Glyde R, et al. Structures of RNA Polymerase Closed and Intermediate Complexes Reveal Mechanisms of DNA Opening and Transcription Initiation. Mol Cell. 2017
46. Zhang X, Wigley DB. The 'glutamate switch' provides a link between ATPase activity and ligand binding in AAA+ proteins. Nature structural & molecular biology. 2008; 15:1223–7.

Europe PMC Funders Author Manuscripts

Europe PMC Funders Author Manuscripts

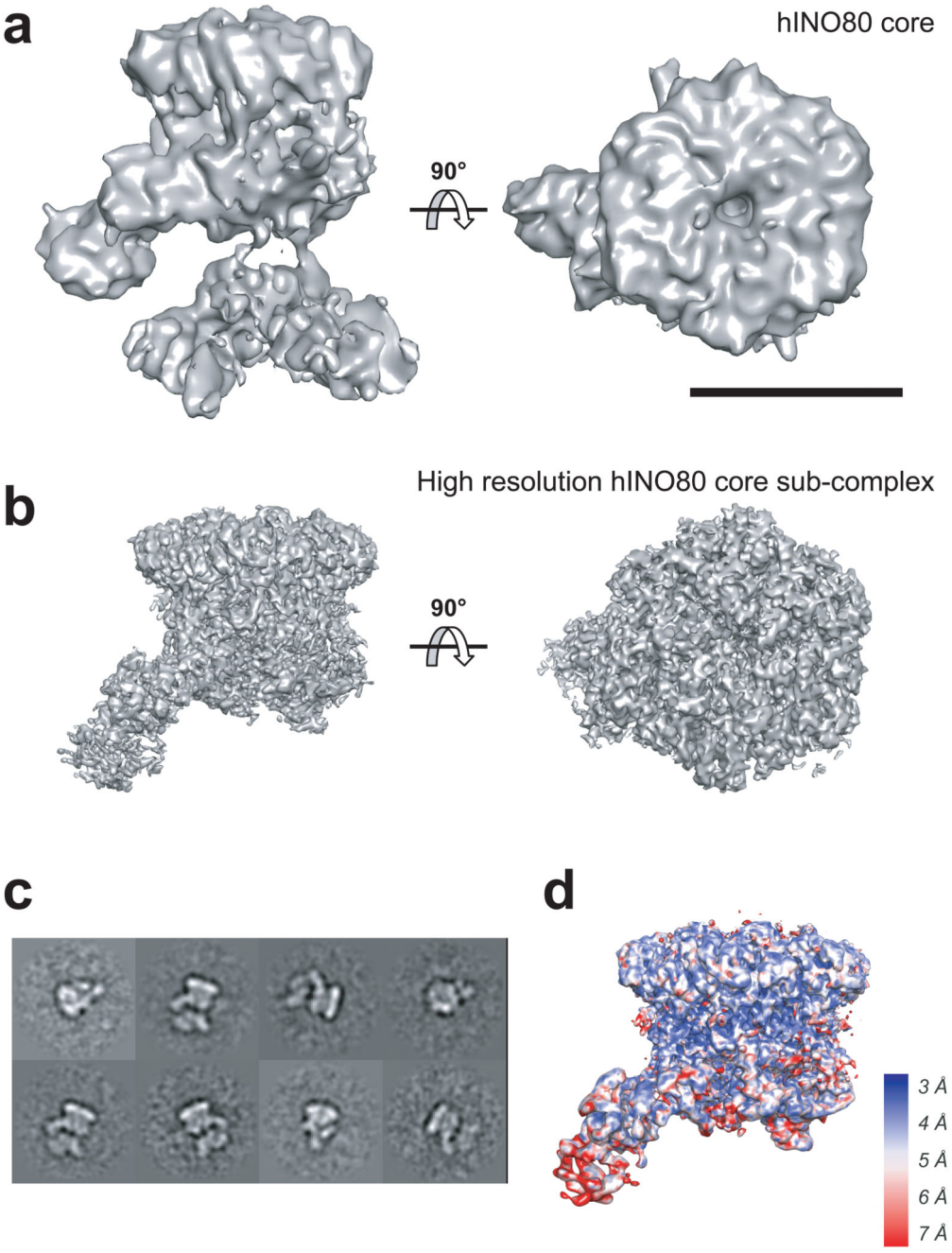

Figure 1. CryoEM reconstructions of various hINO80 complexes.

(a) The 9.6 Å hINO80 core complex. **(b)** The high resolution (4.1Å) hINO80 core sub-complex. The mobile SC1 component is absent. Scale bar: 100 Å **(c)** Examples of 2D classes of particles that display the presence of SC1 and lead to the 9.6 Å structure. **(d)** Local resolution map of the high resolution hINO80 core sub-complex.

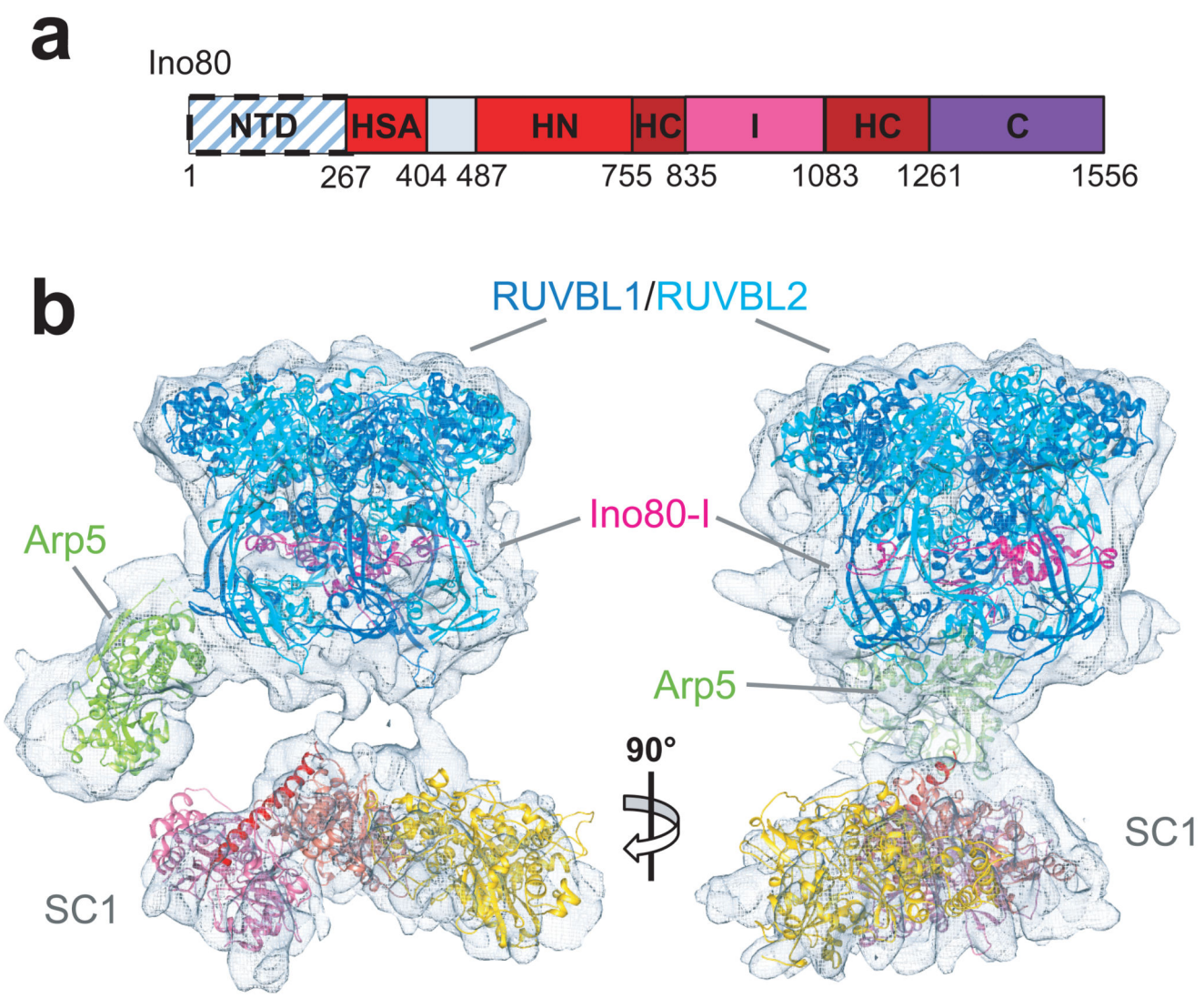

Figure 2. Subunit assignments in the hINO80 core complex.

(**a**) Ino80 domain organisation with functional domains labelled. The N-terminal domain (NTD) is deleted in this study. Colors are used in subsequent figures. **(b)** Subunit assignments with structural models fitted into the hINO80 core complex in two orthogonal views.

Europe PMC Funders Author Manuscripts

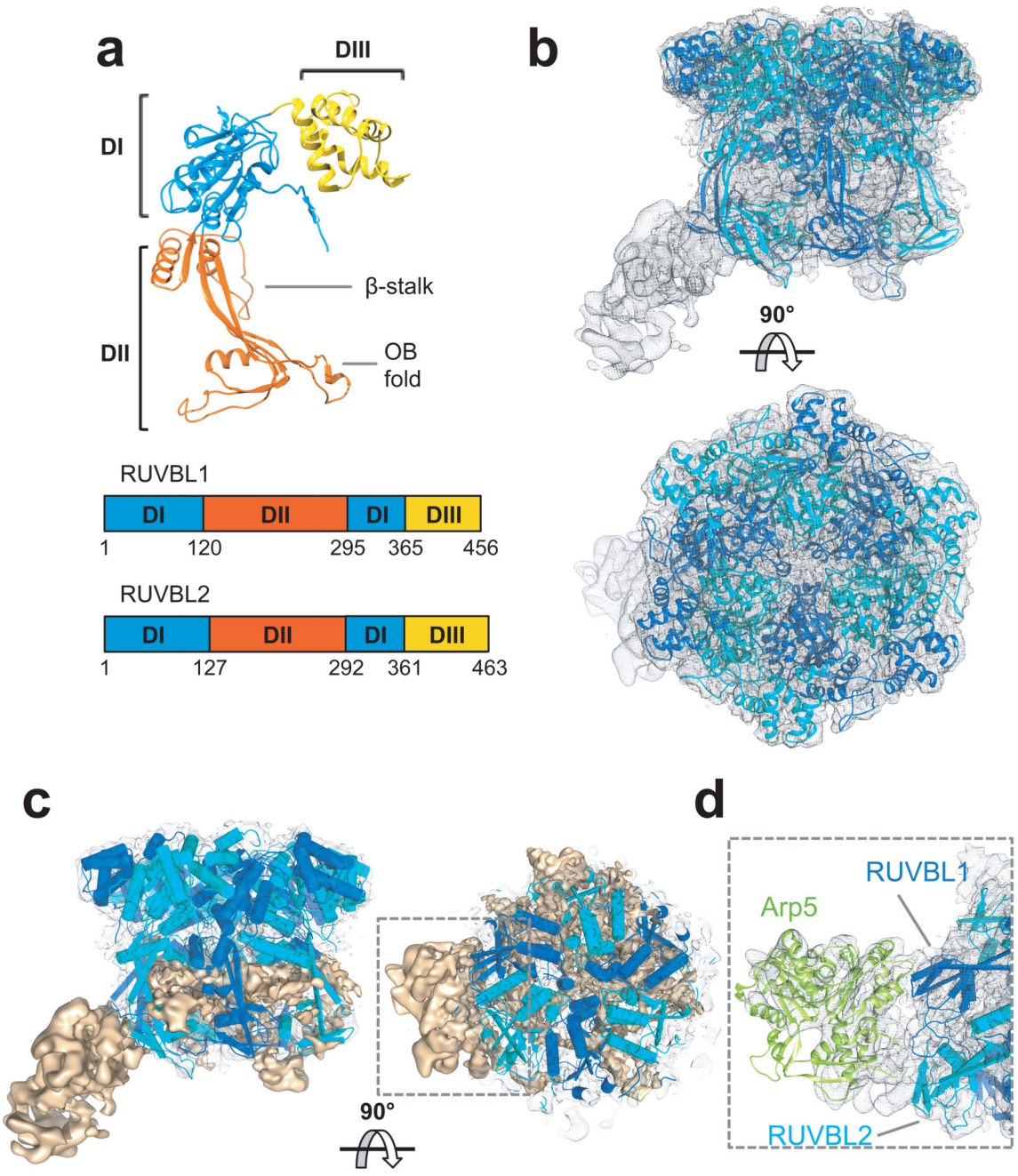

Figure 3. RUVBL1-2 model building into high-resolution hINO80 core complex.

(**a**) RUVBL1-2 domain structures. **(b)** The RUVBL1-2 structural model (RUVBL1 in blue and RUVBL2 in cyan) in the high-resolution hINO80 core sub-complex structure shown in two orthogonal views. **(c)** Difference map between the high-resolution hINO80 core sub-complex and density corresponding to RUVBL1-2, again in two orthogonal views. **(d)** An Arp5 homology model (actin fold, lime) fits nicely into the tail density. Additional density unassigned between the actin fold and that of RUVBL1-2 likely corresponds to Ies6 and/or Arp5 insertions into the Actin fold.

Europe PMC Funders Author Manuscripts

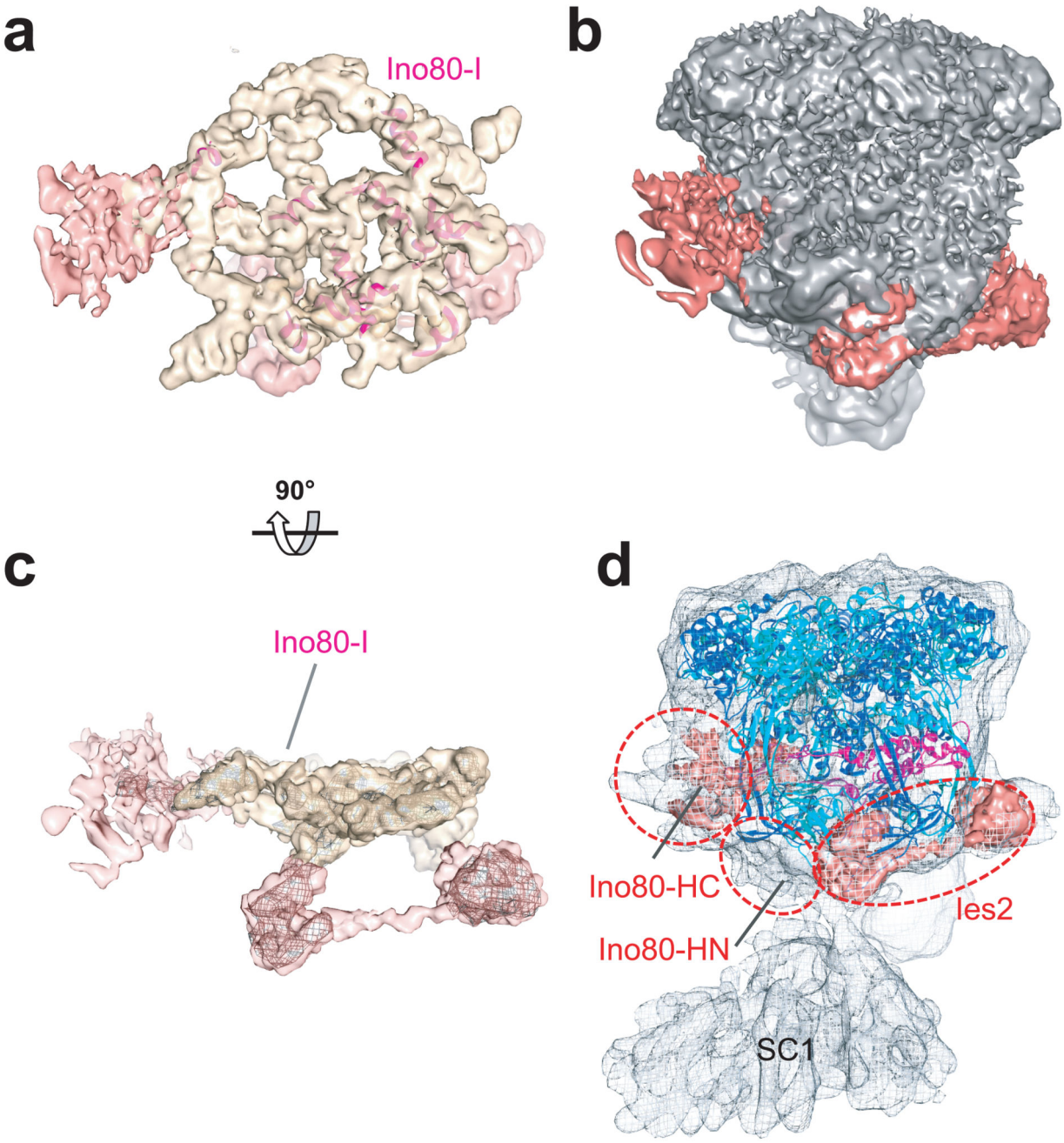

Figure 4. Ino80 subdomains and Ies2 within the high-resolution hINO80 core sub-complex.

(a) Difference map (with RUVBL1-2 subtracted from the hINO80 core sub-complex reconstruction) showing that Ino80-I forms a flat, spoked-wheel structure. A few α-helices have been placed into the density. **(b)** Unassigned density (red) in hINO80 core sub-complex. **(c)** Difference map (solid) as in (**a**) showing that the Ino80-I spoked-wheel is connected to additional density regions which correspond to the unassigned density in (**b**) (red). Shown in grey mesh is the difference map between SC2plus and SC2, which identifies the location of Ies2. (**d**) Ino80-H and Ies2 in the hINO80 core complex.

Europe PMC Funders Author Manuscripts

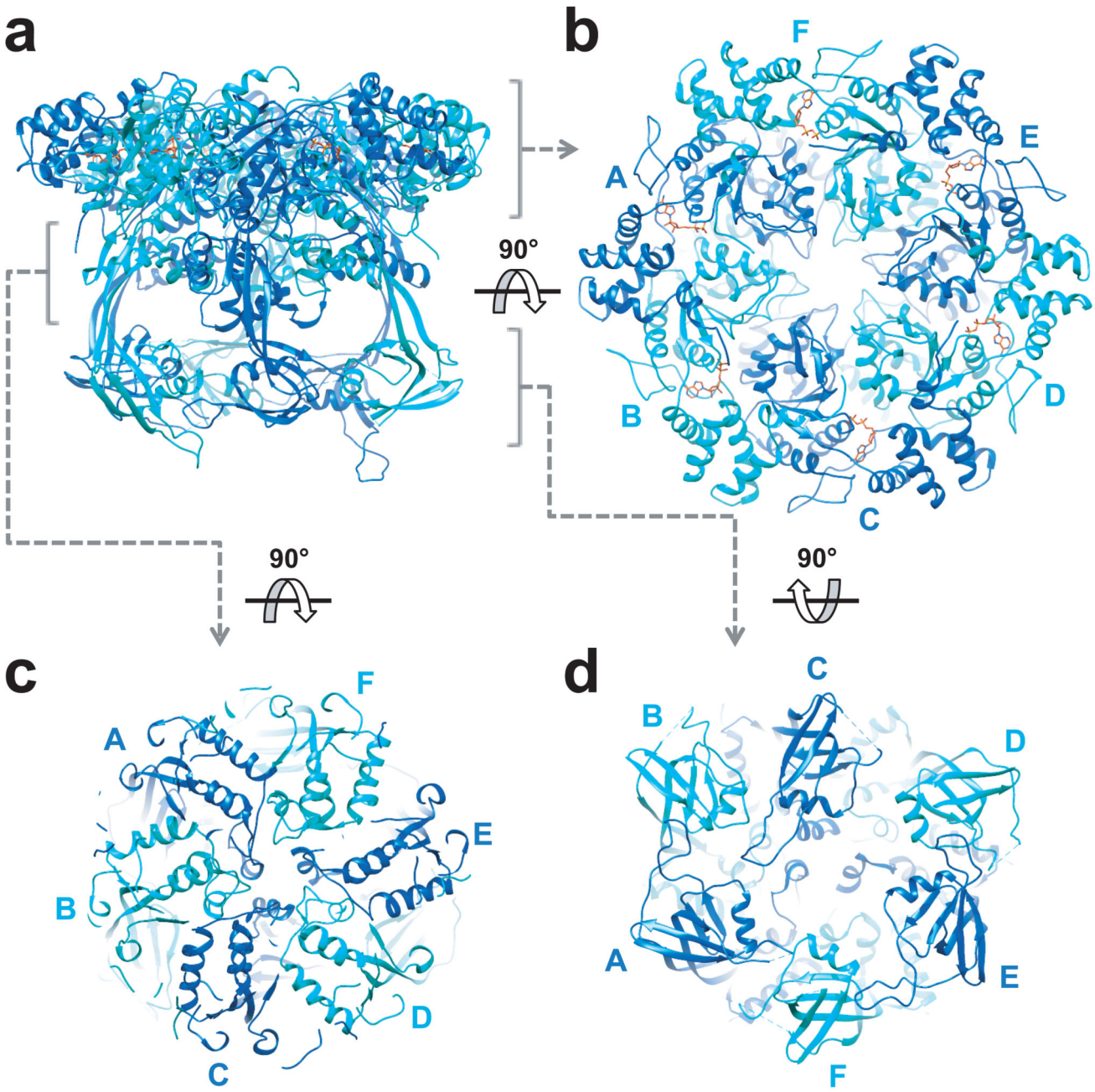

Figure 5. RUVBL1-2 structures in the context of hINO80 core complex.

(a) Side view showing that the RUVBL1-2 heterohexamer forms a barrel consisting of three layers, with all OB domains reaching downwards. **(b)** The top layer consists a planar arrangement of the AAA+ domains with a narrow opening in the middle. **(c)** The middle layer consists of the DII helical bundle and β-stalk that form a plane again with no opening in the centre. **(d)** The bottom layer formed by the OB folds, which deviates from 3-fold symmetry. The large cavity in the centre accommodates the Ino80-I domain. Shown in red sticks are bound ADP molecules.

Europe PMC Funders Author Manuscripts

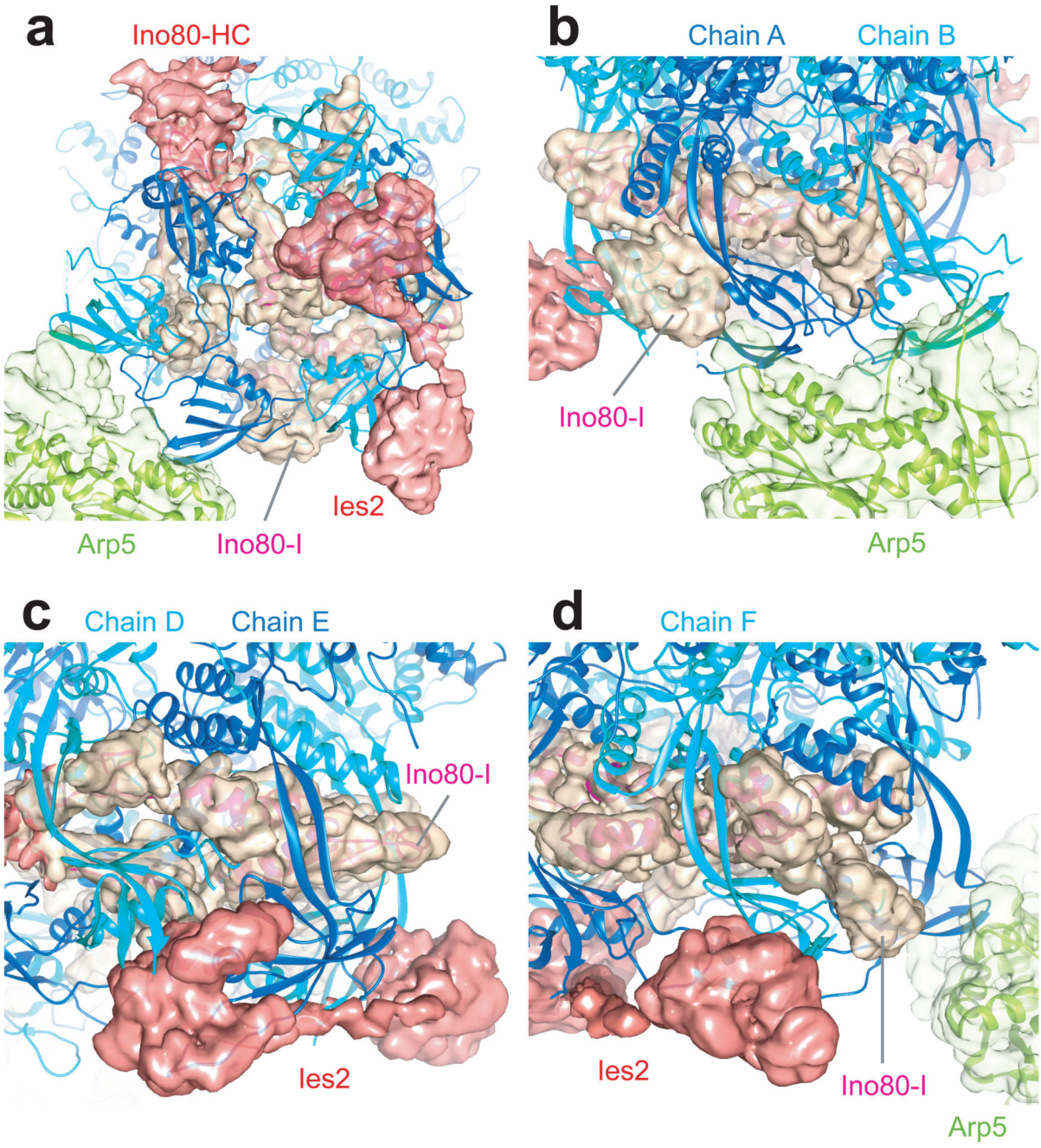

Figure 6. RUVBL1-2 makes extensive and unique interactions.

RUVBL1 (blue) and RUVBL2 (cyan) are shown as ribbons with the difference map as in Fig. 4a shown for other components within the high-resolution hINO80 core complex. **(a)** Bottom view showing the OB folds of RUVBL1-2 making extensive interactions with Ino80-I, Ino80-HC, Ies2 and Arp5-Ies6. **b)-(d)** Each RUVBL1-2 protomer has a unique set of interactions with different domains and/or subunits within the INO80 complex.

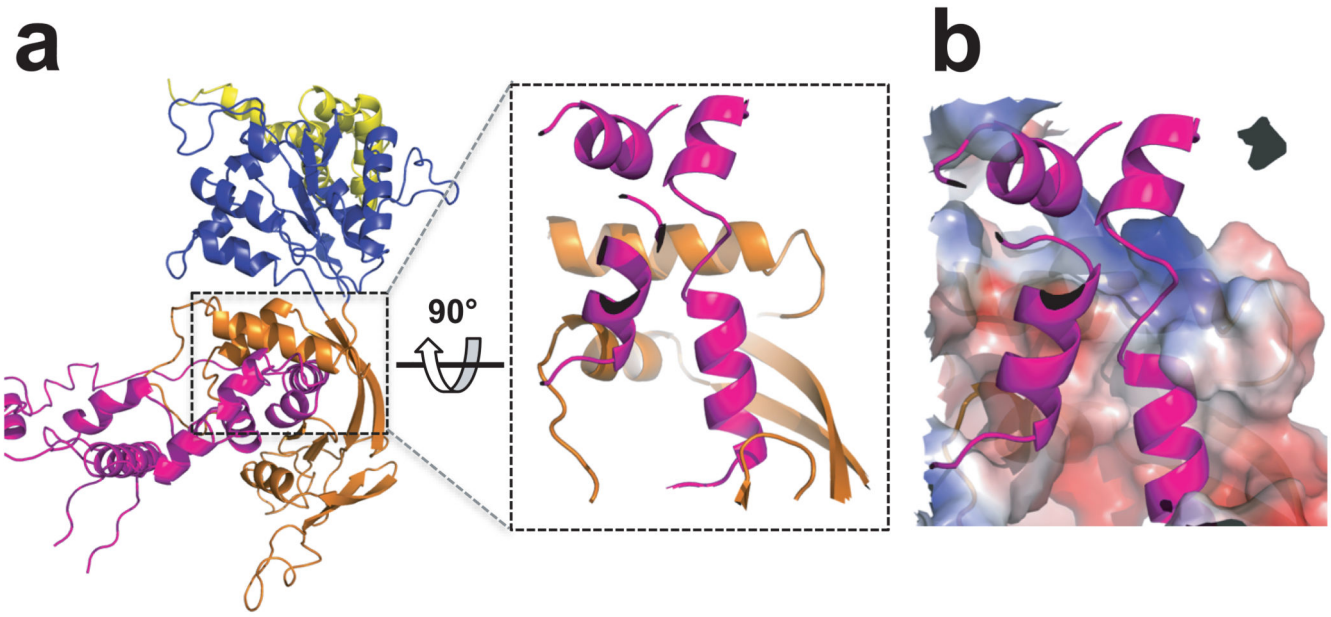

Figure 7. Partner binding cleft in RUVBL1-2.

(a) Ino80-I (magenta) binds to RUVBL1 (chain A) DII cleft (same color scheme as in Fig. 3a). Inset shows the detailed binding cleft involving RUVBL1/2 DII helical bundle and β-stalk. **(b)** Surface potential of the binding cleft containing a hydrophobic core surrounded by charge residues. Blue – positively charge, red – negatively charged, white – hydrophobic residues.

Europe PMC Funders Author Manuscripts

Table 1
Cryo-EM data collection, refinement and validation statistics

	hINO80 core complex (EMD-3772)	High resolution hINO80 sub-complex (EMD-3773 PDB 5OAF)	SC2 (EMD-3774)	SC2plus (EMD-3775)
Data collection and processing				
Magnification	123,000	123,000	62,000	62,000
Voltage (kV)	300	300	200	200
Electron exposure (e–/Å^2)	45-50	45	43	50
Defocus range (μm)	-1.0 to -3.5	-1.2 to -3.2	-1.3 to -4.5	-1.0 to -4.0
Pixel size (Å)	2.26	1.06	3.30	3.30
Symmetry imposed	none	none	none	none
Initial particle images (no.)	367,000	304,304	231,000	96,533
Final particle images (no.)	11,496	104,214	74,226	85,989
Map resolution (Å)	9.6	4.1	11.5	8.4
FSC threshold	0.143	0.143	0.143	0.143
Map resolution range (Å)	~7 to ~15	~3 to ~8	~10 to ~15	~8 to ~11
Refinement				
Initial model used		4WVY		
Model resolution (Å)		4.1		
FSC threshold		0.143		
Model resolution range (Å)		4-8		
Map sharpening *B* factor (Å^2)		-140		
Model composition				
Nonhydrogen atoms		19748		
Protein residues		2,538		
Ligands		6		
B factors (Å^2)				
Protein		75		
Ligand		28		
R.m.s. deviations				
Bond lengths (Å)		0.23		
Bond angles (°)		0.41		
Validation				
MolProbity score				
Clashscore		12.2		
Poor rotamers (%)		0.00		
Ramachandran plot				
Favored (%)		97.6		
Allowed (%)		2.4		
Disallowed (%)		0		